Influence of SCW Processing Parameters on ZnO Nano-Structure Using Both Experimental and CFD Approaches

R. PIOLET *, F. DEMOISSON, A. LEYBROS, M. ARIANE and F. BERNARD

Laboratoire Interdisciplinaire Carnot de Bourgogne (ICB)
Département Nanosciences - Equipe MaNaPI : "Matériaux Nanostructurés: Phénomènes à l'Interface"
UMR 5209 CNRS/Université de Bourgogne
9 Avenue Alain Savary
BP 47 870 21078 DIJON Cedex (France)
e-mail : Romain.Piolet@u-bourgogne.fr
tél : 03.80.39.61.70 / fax : 03.80.39.61.67

ABSTRACT

Different technological applications used metal oxide nanoparticles as main components like sensors, varistors, pigments, fillers, electrography and medical materials. Among all synthesis techniques, Supercritical Water (SCW) synthesis is an eco-friendly process for the production of valuable metal oxide nanoparticles. A continuous hydrothermal production process of nano-oxides in sub- and supercritical conditions has been developed by our team since 2001.
The purpose of this study is to investigate the effect of SCW processing conditions on the synthesis of zinc oxide nanoparticles, such as reaction temperature, pressure, flow rates and inlet concentrations.
To a better understanding of chemical mechanisms (including nucleation and growth of particles) and physical phenomena, three-dimensional reactive multiphasic flow simulation as well as heat transfers has been achieved using Fluent® 6.3 software.
First simulation results give interesting information regarding temperature profiles inside the reactor as well as chemical reaction location. Calculated temperatures are in good agreement with experimental ones. Consequently, such a simulation will allow to establish a correlation between a particle nanostructure and mixing process at a molecular scale.

Keywords: *ZnO, continuous hydrothermal synthesis, supercritical water, nano-particles, CFD simulation.*

INTRODUCTION

Zinc oxide nanoparticles are used in a wide variety of products like cosmetics, textiles, skin lotions [1] or ceramics. In the case of cosmetics, ZnO is more interesting than, for example, titanium dioxide TiO_2 thanks to its properties of UV absorbance [2]. Moreover, ZnO is a n-type semiconductor and can be used as varistors [3], chemical sensors [4], photovoltaic solar cells [5], catalysts [6], piezoelectric and luminescent devices [7], pigments [8] and transducers [9]. In the last years, some studies regarding the phytotoxicity of nanoparticles and their DNA damaging potential in human cells have also been carried out [10, 11].
Various methods have been used to synthesize ZnO nanostructures of controlled size and shape, including precipitation, spray pyrolysis, thermal decomposition and hydrothermal synthesis [12, 13]. Among these techniques, supercritical hydrothermal synthesis ($T > 374$ K and $P < 22.1$ MPa) seems to be the most attractive, due to its perfect control of morphology, purity, cristallinity, composition and low cost for large scale production [14].
In this context, a continuous hydrothermal production process of oxides nanoparticles has been developed in our team since 2001 [15-18]. A validated model of the patented

reactor [16] using CFD has been developed to help the understanding of the nucleation and the growth mechanisms of metal oxides in supercritical water. ZnO material will be chosen as model sample for a fundamental study. Moreover, thermodynamic data are lacking in such medium even if some studies have been carried out regarding the determination of solubility of zinc oxide [19], mechanisms and kinetics of reaction of zinc oxidation under supercritical conditions [20].
The aim of this study is to understand the effects of different processing parameters and to identify their influence on nanoparticle size and morphology.
In this paper, we report the direct synthesis of zinc oxide nanoparticles by precipitation in supercritical water with a continuous apparatus. First of all, major operating parameters effects such as reaction temperature (553-673K), pressure (150-350 bar), flow rates (30-90 $mL.min^{-1}$) and inlet concentrations (outlet acidic/basic pH) are investigated. Then, a three-dimension reactive multiphasic flow Computational Fluid Dynamics (CFD) simulation has been achieved using Fluent® 6.3 software. The developed model allows us to understand chemical mechanisms and hydrodynamics phenomena [18, 21]. Using this model, operating parameters effects on particle size distribution are discussed. Sierra Pallares et al. [22] have proposed a mathematical model for the estimation of average diameter attained by nanoparticles, using population balance model and has shown the dependence of mixing on particle size distribution.

MATERIAL & METHODS

The inlet solutions are prepared by dissolution of zinc nitrate $Zn(NO_3)_2$ (98% pure, from Sigma Aldrich Company) and potassium hydroxide KOH (98% pure, from Sigma Aldrich Company) crystals in de-ionised water.
A schematic of the experimental flow apparatus is shown in Figure 1. Water, zinc nitrate and potassium hydroxide solutions are fed with high pressure membrane pumps at different flow rates. Water is preheated at the desired temperature before the mixing point. The temperature into the reactor is insured by the mean of ceramic furnaces and is determined with type K thermocouples. Operating pressure is maintained by a back-pressure regulator placed after the cooler.

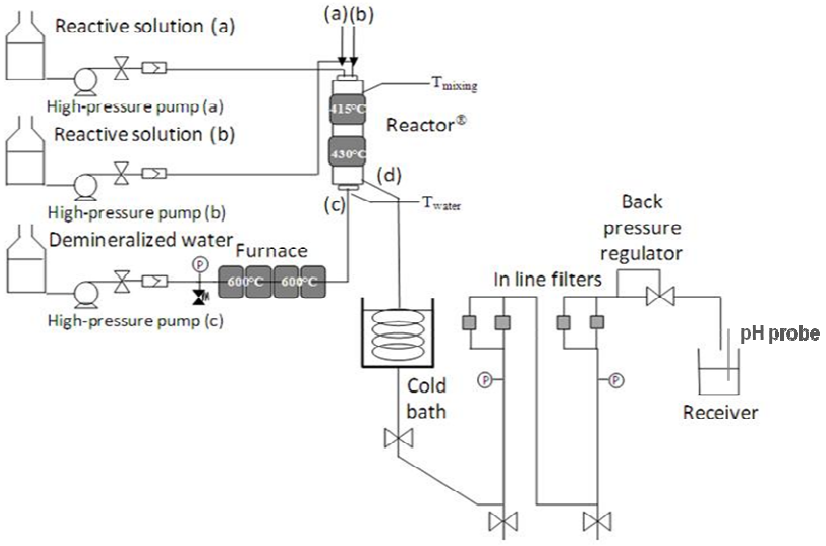

Figure 1 : Schematic of the continuous hydrothermal production process available in the University of Burgundy (Dijon, France) [18]

After reactor outlet, the mixture is quenched thanks to a water cooling bath. Agglomerated particles are removed by in-line filters used to minimize plugging inside the back-pressure regulator.

The reactor is a pipe in pipe concentric arrangement in which the internal pipe has an open ended nozzle with an attached cone [16]. A description of the reactor is given in Figure 2. The reactor is divided in two different areas: the “mixing zone” (where inlet fluids are mixed and where reaction takes place) and the “flowing zone” (zone where the ZnO suspension flows along the external pipe through the reactor). The preheated water is brought through the internal pipe and out the end of the nozzle. Reactant solutions are introduced counter-currently with the preheated water in the mixing zone. The resulted solution is evacuated between the external pipe and the Inconel block. The detailed design of the reactor is presented elsewhere [18].

In the following section, the temperature which will be referred to is the mixing zone temperature. Thermocouple is seated near the reaction zone (as showed in Figure 1) in order to get a representative temperature of reaction medium, called mixing temperature T_{mix}. Indeed, thanks to the preheated water flow, the temperature in the mixing zone could rapidly set to the expected temperature, depending on the pump flows. Operating conditions are summarized in Table 1.

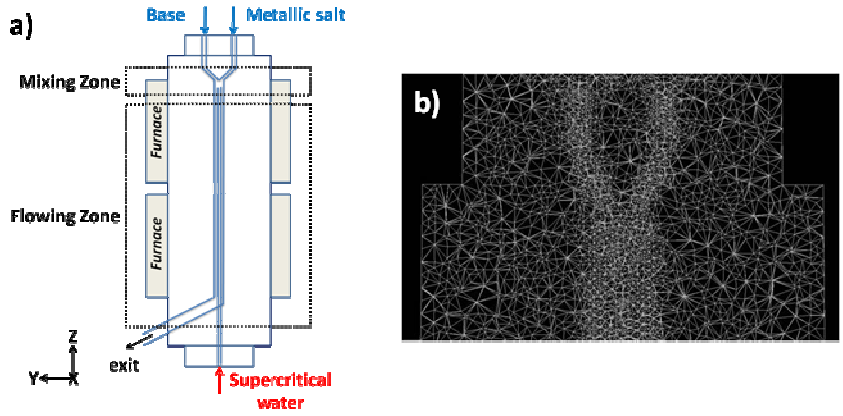

Figure 2 : a) Description of the reactor used for Continuous Hydrothermal Synthesis in sub- and supercritical water, b) Meshing of the reactor around the mixing zone

run	P (MPa)	$T_{measured}$ (K)	Q_{prec} (mL.min^{-1})	Q_{scw} (mL.min^{-1})	Q_{base} (mL.min^{-1})	[ ] / [ ]	pH
1	15	613.5	20	20	20	4	≥ 12
2	30	546.0					
3	30	550.0	20	20	20	0	≈ 1
4		561.6				1	≈ 7
5		537.0				4	≥ 12
6		465.6	20	20	20		
7		563.4					
8		543.8	10	10	10		
9		539.4	20	20	20		
10		512.6	30	30	30	4	≥ 12
11		593.6	15	30	15		
12		426.8	30	10	30		
13		557.3	10	30	30		
14		564.5	30	30	10		

Table 1 : Operating conditions (pressure, mean mixing temperature, flow rates, over-stoichiometry and pH measured in the receiver)

The powders are analysed by X-Ray Diffraction (XRD) to determine the crystallized phase. The size and shape of synthesized nanoparticles is investigated by Transmission Electron Microscopy (TEM). The crystal structures of the end-products are analyzed by powder X-ray Diffraction (XRD) (D8 Vantec, Bruker) using CuK_α radiation.
Transmission electron microscopy (TEM) characterizations of the powders are carried out on Jeol JEM-2100 LaB_6 TEM operating at 200 kV. The TEM observations are performed in bright field mode and the micrographs are acquired and processed thanks to a Gatan US1000 CCD camera and Digital Micrograph software (Gatan, Inc).

RESULTS AND DISCUSSION

1. Experimental results

Using supercritical water hydrothermal synthesis (SCWHS) process, ZnO nanopowders have been synthesized with varying operating parameters. Changes in morphology and particle size distribution (PSD) are obtained depending on those parameters. Effects of pressure (section 1.1), amount of hydroxide ions over Zn(II) ions (section 1.2), temperature (section 1.3) and flow rates (section 1.4) are discussed in the following paragraphs.
All experiments mentioned in Table 1 have been analyzed by XRD measurements and exhibit the same pattern presented in Figure 3, meaning a pure ZnO hexagonal wurtzite crystal structure [23, 24]. A change in 100/002 peaks intensities ratio may be observed, and is assumed to be induced by shear stresses occurring when powders are compacted into the XRD holder, in the case of whiskers-like particles [25].

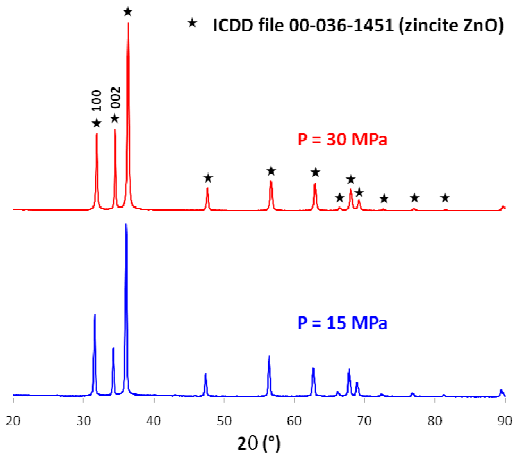

Figure 3 : XRD patterns of ZnO particles prepared by Continuous Hydrothermal Syntheses in sub- (P=15 MPa, run 1) and supercritical water (P=30 MPa, run 2)

1.1 Pressure effect

Experiments have been performed for different values of pressure between 15 and 30 MPa (runs 1 and 2). Transmission electron micrographs show a significant change of the PSD when the pressure increases. Indeed, Figure 4b shows a narrower distribution of small particles not exceeding 200 nm when the pressure increases. This result highlights that pressure is a key operating parameter showing the interest of supercritical water syntheses over sub-critical water syntheses. Syntheses performed at 15 MPa present a mix of micro and nanoparticles with different shapes, whereas at 30 MPa micrographs exhibit nanoparticles with identical whiskers-like shape and with a mean size between 100 and 200 nm, exclusively.

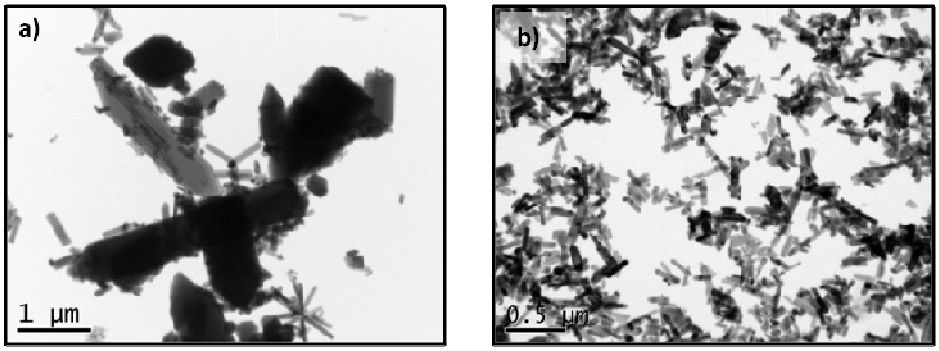

Figure 4 : Evolution of ZnO particles morphology with the pressure a) run 1 P=15 MPa, b) run 2 P=30MPa

Transmission electron micrographs show a tightening of the PSD with an increase of operating pressure from 15 to 30 MPa. This illustrates one of the benefits of supercritical water synthesis since the use of organic precipitating agents is no longer necessary for the production of particles with a uniform morphology.

1.2 Inlet concentrations and pH effects

A preliminary study has been carried out in order to determine the influence of the potassium hydroxide presence in the reactive medium on the zinc oxide crystal growth. In this aim, several experiments (runs 3, 4 and 5) have been performed (Table 1). For technical aspects, the pH cannot be measured inside the reactor, so a pH probe is placed after the back-pressure regulator (Figure 1). Hence, the need of an alkali medium to synthesize nanopowders under supercritical water conditions is discussed.

Transmission electron micrographs reveal that a high excess of HO^- ions in solution enhances the production of smaller sphere-like particles (Figure 5c, run 5). The synthesis of zinc oxide without hydroxide ion presence is possible in supercritical water conditions but is not appropriate for the production of nanoparticles (run 3). Indeed, whiskers with large PSD of around several micrometers are obtained in such conditions and with a low reaction yield (Figure 5a). Figure 5b corresponds to the powder for which the synthesis has been carried out with as much hydroxide ions as zinc ions (run 4). This micrograph reveals that a mix of morphologies is obtained, a large quantity of less than 100 nm whiskers and some sphere-like nanoparticles. The optimized amount of hydroxide ions for the preparation of sphere-like zinc oxide nanoparticles with a narrow PSD has been determined to be $n_{HO^-}/n_{Zn(II)} = 4$, in the case of our patterned reactor.

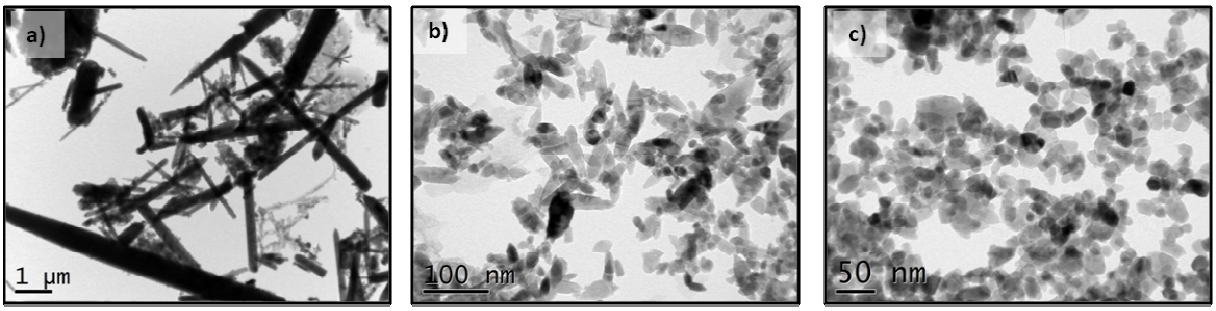

Figure 5 : Evolution of ZnO particles morphology with the reactive solutions concentrations ratio a) run 3 without base, b) run 4 with $[HO^-]/[Zn(II)]=1$ and c) run 5 with $[HO^-]/[Zn(II)]=4$

The need of an alkali medium for the supercritical water synthesis of 20 nm controlled sphere-like particles has been observed. This can be explained by the presence of specific ions in alkali medium. Indeed, the establishment of a predominance diagram for zinc species in

solution would illustrate particle morphology dependency with the pH. Zhang et al. [26, 27] have already established that, at atmospheric pressure, $Zn(OH)_2$ and $Zn(OH)_4^{2-}$ are responsible for the formation of whiskers and star-like particles, respectively. The same study has to be carried out in supercritical water conditions in order to get a better understanding of ZnO particle morphology dependency.

1.3 The mixing temperature effect

In this section, the mixing temperature effect on nanoparticle morphology is investigated. In this purpose, experiments where the mixing temperature is close to 465, 503, 533 and 563K have been carried out (flowing zone temperature remaining around 673K) but only the extreme conditions will be expressed here (465K and 563K, run 6 and 7 respectively). The conditions are summarized in Table 1 but it can be noticed that flow rates are held constant and, only the furnace temperature are tuned to reach the desired conditions.
TEM micrographs corresponding to runs 6 and 7 are presented in Figure 6. Each sample exhibits particles with relatively narrow PSD around 30 nm and sphere-like shape. It appears that an increase of the mixing temperature influences neither the particle morphology nor the PSD.

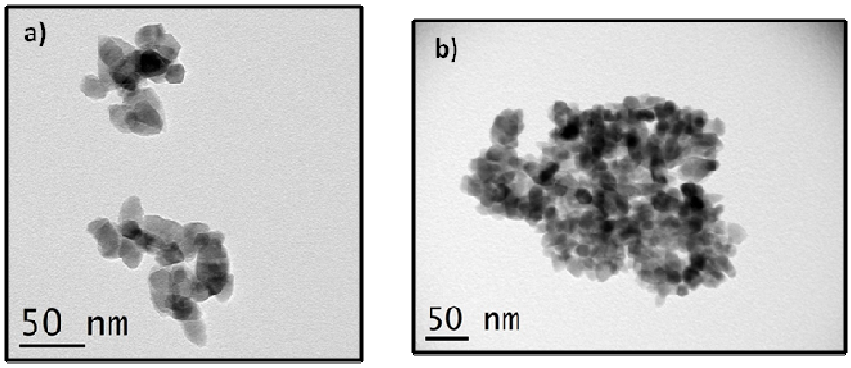

Figure 6 : Evolution of ZnO particles morphology with the mixing temperature a) run 6 Tmix=465K and b) run 7 Tmix=563K

1.4 Flow rates effects

Two sets of experiments were carried out to study the flow rates effects. In the first case, all three flow rates are identical, runs conditions will be referred as “symmetrical” (section 1.4.1). The other case matches with experiments where at least one flow rate is different from the others. Such conditions will be referred as “asymmetrical” (section 1.4.2). In both cases, the mixing temperature has been carefully observed in order to compare those results with CFD results (section 2.3) and, hence determine whether the model is validated or not. The symmetrical flow rates study will allow to understand the effect of residence time inside the reactor on particle morphology. The significance of each flow rate will be investigated in the asymmetrical flow rates study and the flow rates effects on the mixing temperature will be showed.

1.4.1 Symmetrical flow rates

Micrographs in Figure 7 show no modification of the morphology when the residence time estimated thanks to CFD simulation (section 2.3) is below 11 seconds (runs 9 and 10, Figure 7b and c). Sphere-like particles of about 20 nm with a narrow PSD have been synthesized in such conditions. For greater residence time (run 8, Figure 7a), a modification of particle size and morphology is observed. Here, 100 to 200 nm whiskers-like particles have been produced with a slight amount of 30 nm sphere-like particles.

These results are consistent since the particle size increases with the residence time inside the reactor as shown by TEM micrographs. So, residence time seems to be the factor which impacts the particles size.

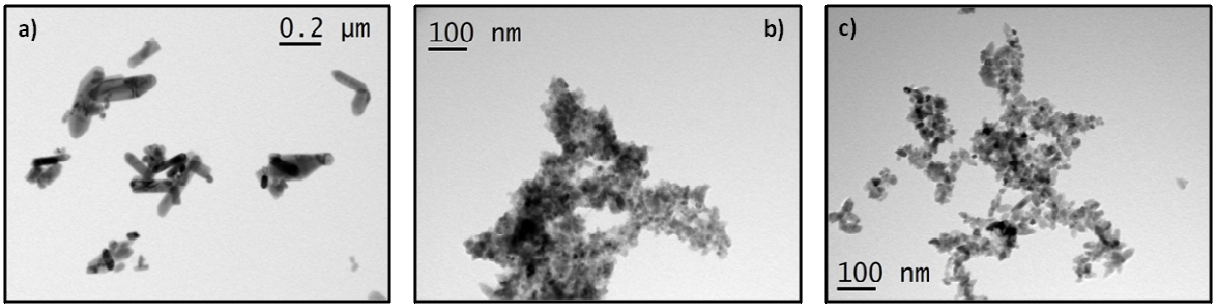

Figure 7 : Evolution of ZnO particles morphology with symmetrical flow rates a) run 8 (10/10/10), b) run 9 (20/20/20) and c) run 10 (30/30/30 mL.min^{-1})

1.4.2 Asymmetrical flow rates

Note that, all comparisons between runs concern only a modification of precursor, water or base flow rate with the conservation of potassium hydroxide over-stoichiometry. Figure 8 presents the micrographs for runs which allow to determine each flow rate effect.

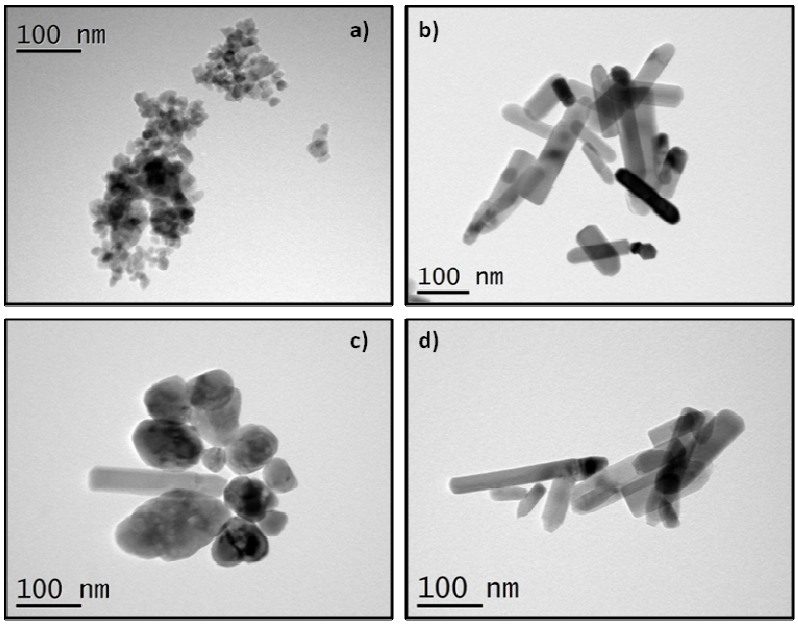

Figure 8 : Evolution of ZnO particles morphology with asymmetrical flow rates a) run 10 30/30/30, b) run 13 10/30/30, c) run 12 30/10/30 and d) run 14 30/30/10 mL.min^{-1} (*metallic salt/SCW/base*)

By comparing micrographs of powders obtained for run 10 and for runs 12, 13 or 14, it is possible to determine the supercritical water, metallic salt and base flow rates effects. But not only these last effects occur. Indeed, there is also a change in the residence time. However, the residence time has previously been considered to have an effect on particle size (section 1.4.1). Thus, it is possible to assign to each effect an influence on particle morphology.

It appears that the conditions of the run 10 (Figure 8a) allow to produce 20 nm sphere-like particles with narrow PSD. Run 13 (Figure 8b) shows the formation of less than 200 nm whiskers-like particles. Hence, the metallic salt flow rate seems to be a factor which influences particle shape.

A great metallic flow rate enhances the formation of sphere-like particles whereas whiskers are produced for a lower flow rate. As for the run 13, run 14 (Figure 8d) presents less than 200 nm whiskers-like particles. So, the base flow rate also appears to have the same effect on particle shape. On the other hand, particles with a size greater than 100 nm and with different morphologies are produced in the conditions of run 12 (Figure 8c). Actually, for this case, another factor has to be taken into account, the temperature effect. A water flow rate change not only modifies the residence time but also the mixing temperature (Table 1) since the water is preheated before the mixing point. Here, three factors are linked: the residence time, the water flow rate and the mixing temperature. For now, the decomposition of these three factors is not quite understood. But it seems that greater water flow rate enhance the particle size and shape control.

2. Simulation results

2.1 Meshing

In order to get information by CFD simulations, the preliminary step is to represent the 3D geometry of the reactor and to divide it in several cells in which all fluid mechanics equations will be solved. This step is carried out thanks to GAMBIT® software. The geometry of the tubular reactor is reported in Demoisson et al. [18]. The built mesh contains about 820,000 cells. Their distribution is refined in the zone of the internal tube to obtain more accurate results (Figure 2b).

2.2 Boundary conditions

Fluid properties at 30 MPa are specified in Fluent® software. This software solves classical mass, momentum and energy conservation equations to describe fluid behaviour and properties. An ideal mixing is assumed. Density and thermal conductivity are calculated by weighted means. The prepared solutions are supposed to be diluted solutions and then, viscosity and specific heat of water are considered. Here, the turbulence is taken into account with the k-ε model [28]. Chemical reactions have been simulated using Eddy Dissipation model [29] by supposing in a first step a monophasic flow. In this model, reaction rates are controlled by the mixing of reactants at a molecular scale. Demoisson and al. [17] proposed a two-step mechanism for the formation of zinc oxide (Eq. 1-2).

$$Zn(NO_3)_2 + 2\,H_2O \rightarrow Zn(OH)_2 + 2\,HNO_3 \qquad \text{Eq. (1)}$$

$$Zn(OH)_2 \rightarrow ZnO + H_2O \qquad \text{Eq. (2)}$$

2.3 Results

CFD simulations have been carried out for every run summarized in Table 1. The observation of temperature, velocity fields, concentrations and turbulent reaction rate profiles in the reactor will give new information as reaction location and formed oxide particle trajectories in mixing and flowing zones. The turbulent reaction rate corresponds to a formation reaction rate based on micromixing and turbulence phenomena. It can be expressed for Eq. (1-2) but the $Zn(OH)_2$ formation of Eq. (1) is assumed to be the limiting reaction for this mechanism. Note that, the turbulent reaction rate is different from nucleation and growth kinetics.

Moreover, this model has been previously validated using mixing temperature measurements [18]. First, temperature, concentration and velocity profiles are presented in the case of the run 5. Then, only the turbulent reaction rate results will be revealed (run 5) to

illustrate morphology changes according to experimental conditions variations. Afterwards, the evolution of the pH and the metallic salt flow rate are investigated in the following section 2.3.2. Links between calculated turbulent reaction rate and particles morphology observed by TEM are discussed. CFD simulation allows to determine the residence time in mixing and flowing zones inside the reactor. Residence time is evaluated to be in the range of 11 seconds considering run 5, 6 seconds (run 10) and 22 seconds (run 8).

2.3.1 Simulated profiles

Figure 9 which presents the temperature profiles in the reactor of the run 5 reveals an inhomogeneous temperature distribution (upper right corner of Figure 9) that is likely due to turbulence and micromixing phenomena which occur in this zone. Indeed, the velocity fields profile in the mixing zone (Figure 10) is in agreement with this assumption since a change of the direction of the velocity fields can be noticed.

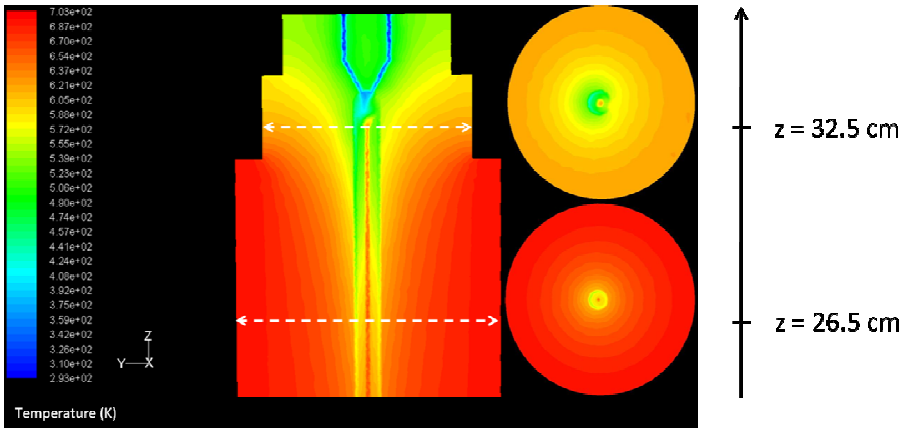

Figure 9 : Axial and transversal temperature profiles in the reactor for the run 5

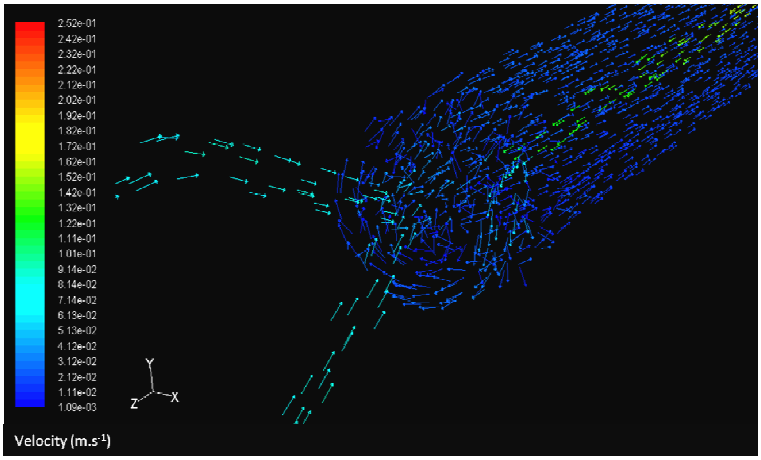

Figure 10 : Velocity fields profile in the mixing zone of the reactor and visualization of the fluids mixing for the run 5

The concentrations of $Zn(NO_3)_2$, KOH, $Zn(OH)_2$ and ZnO species and turbulent reaction rate profiles presented in Figure 11 and Figure 12, respectively, allow to point out the ZnO formation reaction location. The reaction is located at the outlet of the metallic salt injection pipe for the run 5. The next step of the study would be to correlate the turbulent reaction rate value with the particle morphology. Thus, the simulation would be a predictive tool for synthesized particle morphology determination from operating parameters variations.

2.3.2 Calculated turbulent rate profiles and correlation with observed particle morphologies

As said earlier, the turbulent reaction rate profiles are investigated considering pH evolution (runs 4 and 5) and precursor flow rate variation (runs 13 and 10). Both parameters have been experimentally determined to have an effect on the morphology (see Figures 5, 7 and 8). For each parameter, two particles shapes can be observed depending on operating conditions: sphere-like particles and whiskers. An evaluation of the turbulent reaction rate values would allow to predict these morphologies. Indeed, a modification of the turbulent reaction rate profile is observed when the outlet pH varies from neutral (pH ≈ 7, run 4) to strongly alkali (pH ≥ 12, run 5). There is a significant change in the reaction rate value, by a factor of 2 in neutral medium. This different reaction rate value can explain the formation of larger particles in neutral medium. A change in the reaction location can also be noticed and correlated with the lack of hydroxide ions. On the other hand, simulation reveals that for the run 5, the reaction occurs at the outlet of the metallic salt flow rate which is consistent with an excess of hydroxide ions.

For a metallic salt flow rate modification, a decrease by a factor 2 of the turbulent reaction rate value is observed. There is no noticeable shift of the reaction location inside the mixing zone. As for the previous case, experiments where the value is the lowest correspond to whiskers whereas sphere-like particles are observed for a greater turbulent reaction rate.

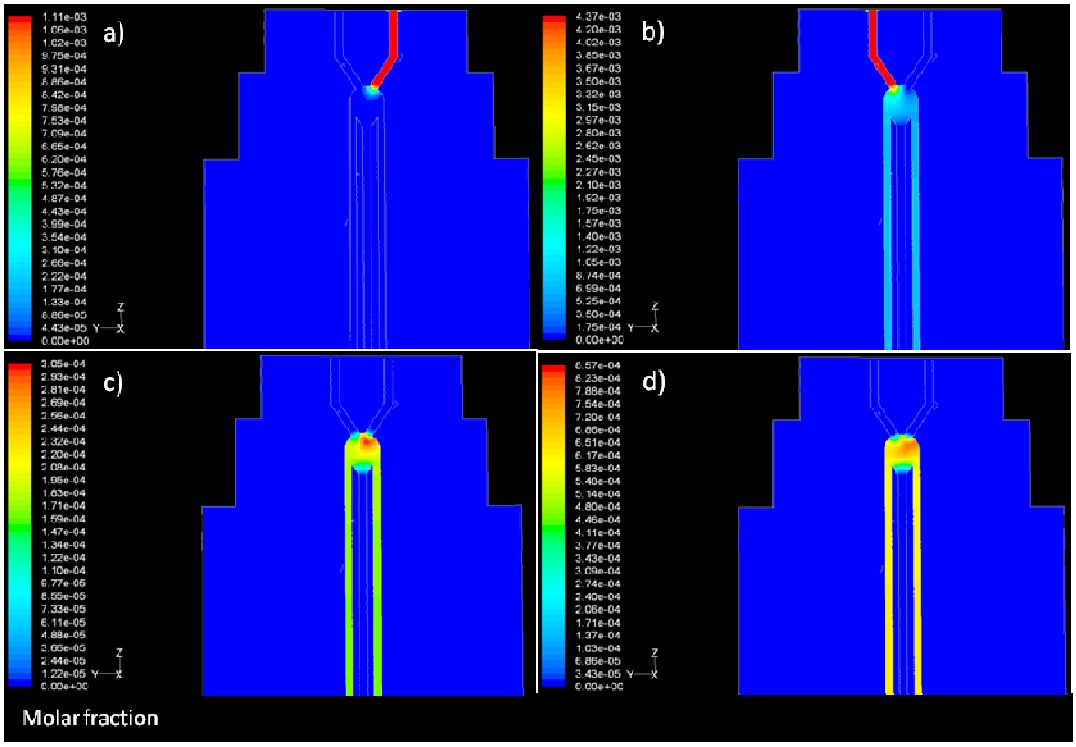

Figure 11 : Concentration profiles of different species a) $Zn(NO_3)_2$, b) KOH, c) $Zn(OH)_2$ and d) ZnO around the mixing zone during the reaction for run 5

Micrographs and CFD simulations show that the metallic salt flow rate is an important operating parameter which rules particle morphology by modifying the turbulent reaction rate.

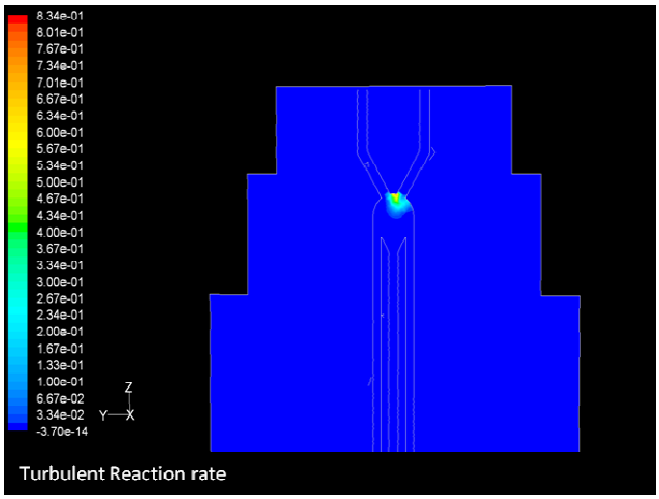

Figure 12 : Turbulent Reaction rate profile calculated for the Eq. (1) and for run 5

Concerning the turbulent reaction rate, a pattern has been identified for the evolution of this value with particle morphologies. Indeed, sphere-like particles are observed when the reaction rate is close to 1 whereas a value of approximately 0.4 matches with whiskers. So, running simulations and identifying the corresponding turbulent reaction rate are the first step of the morphology prediction for the synthesis of zinc oxide nanoparticles in supercritical water.

CONCLUSION

The possibility to synthesize zinc oxide with our continuous supercritical water process has been established. Then, the particles synthesis with different morphologies has been observed and the effects of SCW-processing parameters on those morphologies have been discussed. For that, CFD simulations have been run and correlated with morphologies observed by transmission electron microscopy.

The pressure, the pH and the metallic salt flow rate have been identified to have major impacts on particle morphology unlike the temperature. Indeed, by tuning these operating parameters, sphere-like particles or whiskers have been produced. The effect of precursors chemistry on particle morphology is currently studied. The replacement of zinc nitrate with zinc acetate or sulphate and potassium hydroxide with sodium or lithium hydroxide is considered. The first results tend to show a high sensitivity of particle morphology with the precursor chemistry.

The first aspect of the morphology prediction has been expressed by the determination of turbulent reaction rate value. An optimization of the prediction can be considered with the integration in the simulation of a balance population model for the determination of particle size.

ACKOWLEDGEMENTS

This work is financially supported by the “Conseil Général de Bourgogne” and the OSEO organization. The authors are grateful to the Department of Analysis and Instrumentation (DAI) of the ICB for their assistance in the process development and material characterization.

REFERENCES

[1] NG, C.-T., LI, J.J., BAY, B.-H., YUNG, L.-Y.L., Journal of Nucleic Acids, Vol. 2010, **2010,** p. xxx.
[2] TRAN, D.T., SALMON, R., Australasian Journal of Dermatology, Vol. 52, **2011,** p. 1.
[3] NAHM, C.-W., PARK, C.-H., Journal of Materials Science, Vol. 35, **2000,** p. 3037.

[4] MOCHINAGA, R., YAMASAKI, T., ARAKAWA, T., Sensors and Actuators B: Chemical, Vol. 52, **1998,** p. 96.
[5] GAL, D., HODES, G., LINCOT, D., SCHOCK, H.W., Thin Solid Films, Vol. 361-362, **2000,** p. 79.
[6] ELSEVIERS, W.F., VERELST, H., Fuel, Vol. 78, **1999,** p. 601.
[7] FUJIHARA, S., NAITO, H., KIMURA, T., Thin Solid Films, Vol. 389, **2001,** p. 227.
[8] SIGOLI, F.A., DAVOLOS, M.R., JAFELICCI, M., Journal of Alloys and Compounds, Vol. 262-263, **1997,** p. 292.
[9] ZAYER, N.K., GREEF, R., ROGERS, K., GRELLIER, A.J.C., PANNELL, C.N., Thin Solid Films, Vol. 352, **1999,** p. 179.
[10] KUMARI, M., KHAN, S.S., PAKRASHI, S., MUKHERJEE, A., CHANDRASEKARAN, N., Journal of Hazardous Materials, Vol. 190, **2011,** p. 613.
[11] SHARMA, V., SHUKLA, R.K., SAXENA, N., PARMAR, D., DAS, M., DHAWAN, A., Toxicology Letters, Vol. 185, **2009,** p. 211.
[12] NICHIPORENKO, O.S., Poroshkovaya Metallurgiya, Vol. 252, **1986,** p. 46.
[13] SØNDERGAARD, M., BØJESEN, E.D., CHRISTENSEN, M., IVERSEN, B.B., Crystal Growth & Design, Vol. xxx, **2011,** p. xxx.
[14] HAYASHI, H., HAKUTA, Y., Materials, Vol. 3, **2010,** p. 3794.
[15] AIMABLE, A., MUHR, H., GENTRIC, C., BERNARD, F., LE CRAS, F., AYMES, D., Powder Technology, Vol. 190, **2009,** p. 99.
[16] AYMES, D., ARIANE, M., BERNARD, F., MUHR, H., DEMOISSON, F., Inpi, France, 09 55023, **07/2009.**
[17] DEMOISSON, F., ARIANE, M., PIOLET, R., BERNARD, F., Advanced Engineering Materials, Vol. 13, **2011,** p. 487.
[18] DEMOISSON, F., ARIANE, M., LEYBROS, A., MUHR, H., BERNARD, F., The Journal of Supercritical Fluids, Vol. xxx, **In Press, *Corrected Proof*,** p. xxx.
[19] PLYASUNOV, A., BELONOZHKO, A., IVANOV, I., KHODAKOVSKIY, I., Geochemistry International, Vol. 25, **1988,** p. 77.
[20] VOSTRIKOV, A.A., FEDYAEVA, O.N., SHISHKIN, A.V., SOKOL, M.Y., The Journal of Supercritical Fluids, Vol. 48, **2009,** p. 161.
[21] LESTER, E., BLOOD, P., DENYER, J., GIDDINGS, D., AZZOPARDI, B., POLIAKOFF, M., The Journal of Supercritical Fluids, Vol. 37, **2006,** p. 209.
[22] SIERRA-PALLARES, J., MARCHISIO, D.L., ALONSO, E., PARRA-SANTOS, M.T., CASTRO, F., COCERO, M.J., Chemical Engineering Science, Vol. 66, **2011,** p. 1576.
[23] LOUER, D., AUFFREDIC, J.P., LANGFORD, J.I., CIOSMAK, D., NIEPCE, J.C., Journal of Applied Crystallography, Vol. 16, **1983,** p. 183.
[24] LANGFORD, J.I., BOULTIF, A., AUFFREDIC, J.P., LOUER, D., Journal of Applied Crystallography, Vol. 26, **1993,** p.
[25] OHARA, S., MOUSAVAND, T., UMETSU, M., TAKAMI, S., ADSCHIRI, T., KUROKI, Y., TAKATA, M., Solid State Ionics, Vol. 172, **2004,** p. 261.
[26] ZHANG, H., YANG, D., JI, Y.J., MA, X.Y., XU, J., QUE, D.L., The Journal of Physical Chemistry B, Vol. 108, **2004,** p. 3955.
[27] ZHANG, H., YANG, D., MA, X.Y., JI, Y.J., XU, J., QUE, D.L., Nanotechnology, Vol. 15, **2004,** p. 622.
[28] JONES, W.P., LAUNDER, B.E., International Journal of Heat and Mass Transfer, Vol. 15, **1972,** p. 301.
[29] MAGNUSSEN, F., 19th AIAA Science Meeting, Saint-Louis (USA), **1981**